ELSEVIER

Fluid Dynamics Research 20 (1997) 143–156

FLUID DYNAMICS RESEARCH

# Simulations of dispersed turbulent multiphase flow

M.R. Maxey [a,*,1], B.K. Patel [a], E.J. Chang [b], L.-P. Wang [c]

[a] *Center for Fluid Mechanics, Turbulence and Computation, Brown University, Box 1966, 37 Manning Street, Providence, RI 02912, USA*

[b] *Naval Research Laboratory, Code 6410, Washington, DC 20375, USA*

[c] *Department of Mechanical Engineering, University of Delaware, Newark, DE 19716, USA*

**Abstract**

Direct numerical simulations of homogeneous isotropic turbulence are used to investigate the effects of turbulence on the transport of particles in gas flows or bubbles in liquid flows. The inertia associated with the bubbles or the particles leads to locally strong concentrations of these in regions of instantaneously strong vorticity for bubbles or strain-rate for particles. This alters the average settling rates and other processes. If the mass-loading of the dispersed phase is significant a random "turbulent" flow is generated by the particle settling. A simple demonstration of this is given, showing the statistically axisymmetric character of this flow and how it can modify an ambient turbulent flow.

*PACS:* 47.55.K; 47.27.Q

*Keywords:* Multiphase flow; Turbulent diffusion

## 1. Introduction

Homogeneous turbulence is an important flow to consider in the development of turbulence models. It provides a simple test for the representations of turbulence decay and production without the complications of rigid wall boundaries or mean flow variations. Further homogeneous turbulence is characteristic of the small-scale, dissipation range dynamics of general high Reynolds number turbulent flows. This makes it especially valuable in the study of dispersed two-phase flow where the interactions of the particle phase with small-scale turbulence are still not well understood. Direct numerical simulations have been used for some time to investigate the transport of particles in homogeneous turbulence, one of the earliest studies being by Riley and Patterson (1974). These have been followed by Squires and Eaton (1991a, b), Elghobashi and Truesdell (1992) and Wang

* Corresponding author.

[1] E-mail: maxey@cfm.brown.edu.



*PII* S0169-5983(96)00042-1

and Maxey (1993a) amongst others. Further work for small bubbles has been done by Wang and Maxey (1993b) and Maxey et al. (1994).

As the mass loading of solid particles in a gas flow is increased, or the void fraction of bubbles in water, the turbulence may be modified due to the two-way coupling between the continuous and dispersed phase. Squires and Eaton (1990) and Elghobashi and Truesdell (1993) have investigated this process for homogeneous turbulence in gas–solid flows and found that as the mass loading is increased the turbulence decays more rapidly with an increase in the high-frequency content of the energy spectrum, consistent with available experimental information (Gore and Crowe, 1991). Fundamental information regarding bubbles in homogeneous turbulence comes at present from experiments such as those reported by Lance and Bataille (1991).

In this short paper, we outline some of the issues involved in the particle transport problem (one-way coupling) and the turbulence modification at higher mass loadings (two-way coupling).

## 2. Particle motion

The equation of motion for a small spherical particle in a gas–solid flow may be approximated by a balance of particle inertia and weight against the quasisteady drag force exerted by the surrounding fluid. The velocity $\boldsymbol{V}(t)$ and the position $\boldsymbol{Y}(t)$ of a particle are then given by

$$\frac{\mathrm{d}\boldsymbol{V}}{\mathrm{d}t} = (\boldsymbol{u}(\boldsymbol{Y},t) - \boldsymbol{V}(t) + \boldsymbol{W})/\tau_\mathrm{p}. \tag{1}$$

The particle response time $\tau_\mathrm{p}$ for a small particle of diameter $d$ is

$$\tau_\mathrm{p} = (\rho_\mathrm{p}/\rho_\mathrm{a})(d^2/18\nu), \tag{2}$$

provided a Stokes drag law may be assumed. The terminal settling velocity in still fluid $\boldsymbol{W}$ is $\tau_\mathrm{p}\boldsymbol{g}$, where $\boldsymbol{g}$ is the acceleration due to gravity. The particle density $\rho_\mathrm{p}$ is generally much greater than the density of the gas or air $\rho_\mathrm{a}$, typically by a factor of $10^3$ or more. The kinematic viscosity of the air is $\nu$ and the fluid velocity field is $\boldsymbol{u}(\boldsymbol{x},t)$. This approach is suitable for particles less than 50 $\mu$m or so in diameter and is easily modified to include nonlinear drag forces for slightly larger particles.

In a liquid or water flow containing small bubbles the influence of added-mass must be included and possibly other forces such as lift forces or the effects of history terms. Surfactants will quickly coat a small bubble and make it respond as a massless rigid spherical inclusion. A suitable equation for the motion of a small bubble is

$$0 = m_\mathrm{F}\left(\frac{\mathrm{D}\boldsymbol{u}}{\mathrm{D}t} - \boldsymbol{g}\right) + \frac{1}{2}m_\mathrm{F}\left(\frac{\mathrm{D}\boldsymbol{u}}{\mathrm{D}t} - \frac{\mathrm{d}\boldsymbol{V}}{\mathrm{d}t}\right) + 3\pi d\mu(\boldsymbol{u}(\boldsymbol{Y},t) - \boldsymbol{V}), \tag{3}$$

which represents a balance of the forces due to the ambient flow stresses and buoyancy, added mass and viscous drag. The mass of fluid displaced by a bubble is $m_\mathrm{F}$ and $\mathrm{D}\boldsymbol{u}/\mathrm{D}t$ is the local Lagrangian fluid acceleration. From (3) the working equation of motion is

$$\frac{\mathrm{d}\boldsymbol{V}}{\mathrm{d}t} = (\boldsymbol{u}(\boldsymbol{Y},t) - \boldsymbol{V}(t) + \boldsymbol{W})/\tau_\mathrm{B} + 3\frac{\mathrm{D}\boldsymbol{u}}{\mathrm{D}t}, \tag{4}$$

and $\tau_B$ is the bubble response time scale equal to $d^2/36\nu$. In this context $\boldsymbol{W}$ is the terminal rise velocity, equal to $-2\tau_B\boldsymbol{g}$.

A key issue in calculating the transport of particles or bubbles in a turbulent flow is to determine $\boldsymbol{u}(\boldsymbol{Y},t)$, the local fluid velocity. It should be remembered that in deriving (1) and (4) that the particle is assumed to be small compared to the shortest length scale on which the ambient flow varies. The presence of the particle introduces an additional local disturbance flow whose effect is fully parameterized by the drag force, etc. (Maxey and Riley, 1983). The velocity $\boldsymbol{u}(\boldsymbol{Y},t)$ is that of the ambient flow in the absence of the particle.

## 3. One-way coupling

To investigate the effect of turbulence on instantaneous particle concentrations and mean statistics we have used (1) and (4) in conjunction with direct numerical simulations of homogeneous isotropic turbulence. The flow $\boldsymbol{u}(\boldsymbol{x},t)$ is computed by a pseudo-spectral method assuming periodic boundary conditions and a Fourier series representation of the form

$$\boldsymbol{u}(\boldsymbol{x},t)=\sum_{k}\hat{\boldsymbol{u}}(\boldsymbol{k},t)\exp(\mathrm{i}\boldsymbol{k}\cdot\boldsymbol{x}). \tag{5}$$

The computational domain has side $2\pi$ and the wave number components $k_i$ are integers, $-N/2 < k_i \leqslant N/2$, on a grid of $N^3$ points. The flow is given by

$$\frac{\partial \boldsymbol{u}}{\partial t}=\boldsymbol{u}\times\boldsymbol{\omega}-\boldsymbol{\nabla}\left(p/\rho+\tfrac{1}{2}\boldsymbol{u}^2\right)+\nu\nabla^2\boldsymbol{u}+\boldsymbol{h}(\boldsymbol{x},t), \tag{6}$$

$$\boldsymbol{\nabla}\cdot\boldsymbol{u}=0, \tag{7}$$

where $\boldsymbol{\omega}$, $p$ denote the fluid vorticity and pressure. The term $\boldsymbol{h}(\boldsymbol{x},t)$ included in (6) is a random body forcing term, restricted to very low wave numbers, that provides an energy source to sustain the homogeneous turbulence. By this means stationary homogeneous turbulence can be maintained that will not significantly modify the higher wave number small-scale dynamics. Further details are given by Wang and Maxey (1993a).

These simulations reveal several features. With a $96^3$-grid, $\mathrm{Re}_\lambda = 62$ can be sustained. The turbulence dissipation range can be characterized by the Kolmogorov velocity and time scales

$$v_K=(\varepsilon\nu)^{1/4}, \qquad \tau_K=(\nu/\varepsilon)^{1/2},$$

where $\varepsilon$ is the rate of turbulent kinetic energy dissipation. The velocity gradients contributing to the dissipation dynamics are the most intense, and $\tau_K$ is the shortest time scale of the flow. For $\tau_p/\tau_K \ll 1$ the particles (or bubbles) respond fully to the turbulence fluctuations. An initial, statistically uniform distribution of particles will remain uniform and velocity moments such as the mean settling rate are unaltered. Note that there is no feedback mechanism of the particles on the flow nor are there interaction effects between the particles in this limit of negligible mass loading or void fraction for one-way coupling.

As $\tau_p/\tau_K$ increases inertial effects or added-mass become significant. Even if uniformly distributed initially, particles and bubbles will tend to become concentrated locally. Solid particles will tend

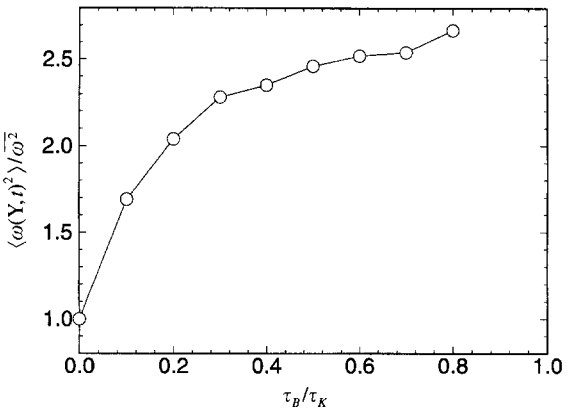


Fig. 1. Ratio of bubble average $\langle\omega^2(\boldsymbol{Y},t)\rangle$ to Eulerian mean square value $\overline{\omega^2}$ as $\tau_B/\tau_K$ varies, $W = v_K$.

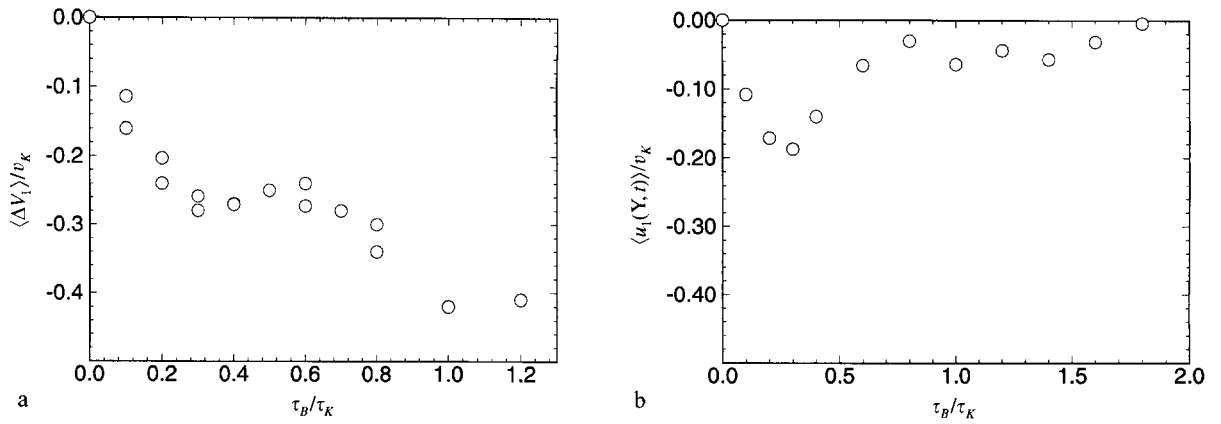


Fig. 2. Changes in mean bubble rise velocity, as $\tau_B/\tau_K$ varies with $W = v_K$ held constant: (a) $\langle\Delta V_1\rangle/v_K = (\langle V_1\rangle - W)/v_K$; (b) $\langle u_1(\boldsymbol{Y},t)\rangle/v_K$. Axes chosen with $\boldsymbol{g} = (-g, 0, 0)$.

to collect in regions of high strain-rate and low vorticity while bubbles show the opposite trend. The concentration of bubbles seems to be a somewhat stronger effect, and the average $\langle\omega^2(\boldsymbol{Y},t)\rangle$ measured at the bubble locations is easily 2 or 3 times the Eulerian mean square value $\overline{\omega^2}$. This is illustrated by the results in Fig. 1 which shows values of this ratio increasing from one as the time scale ratio for the bubbles $\tau_B/\tau_K$ increases, the terminal rise speed is held constant with $W$ equal to $v_K$. This bias has an effect on the average rise velocity of the bubbles $\langle\boldsymbol{V}\rangle$ even if, as here, the Eulerian mean flow $\bar{\boldsymbol{u}}$ is zero. In fact, there is a net reduction in the average rise velocity as shown by the values of $\langle\Delta\boldsymbol{V}\rangle = (\langle\boldsymbol{V}\rangle - \boldsymbol{W})$ shown in Fig. 2 for the same range of bubble parameters. This reduction may be 40% or more. The ensemble average of (4) indicates that the equilibrium value of $\langle\Delta\boldsymbol{V}\rangle$ is governed by contributions from $\langle\boldsymbol{u}(\boldsymbol{Y},t)\rangle$ and $3\tau_B\langle D\boldsymbol{u}/Dt\rangle$. Results for the former are also given in Fig. 2 and this is the main factor at low values of $\tau_B/\tau_K$ while the latter becomes increasingly significant at larger values.

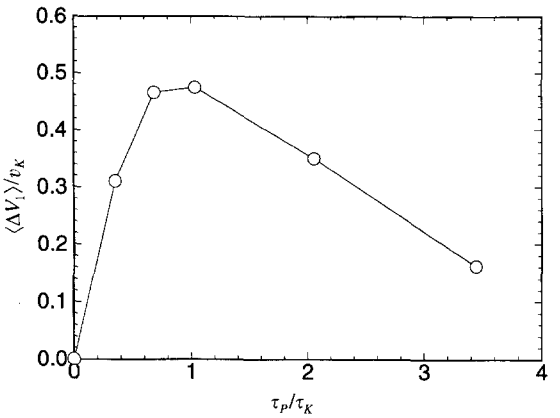


Fig. 3. Changes in mean particle settling velocity $\langle \Delta V_1 \rangle / v_K = (\langle V_1 \rangle - W)/v_K$ as $\tau_p/\tau_K$ varies with $W = v_K$ held constant. Axes chosen with $\boldsymbol{g} = (g, 0, 0)$.

For solid particles the bias mechanism leads to an increase in the mean settling velocity. This increase $\langle \Delta V \rangle$, scaled by $v_K$, is shown in Fig. 3 for particle response times $\tau_p$ varying up to 3.5 $\tau_K$. From (1) this increase is due solely to the net mean value of $\langle \boldsymbol{u}(\boldsymbol{Y}, t) \rangle$ which is greatest around $\tau_p = \tau_K$. It is interesting to note that the small-scale turbulence governs this effect on particles and bubbles, while the more usual questions of dispersion are dominated by the large-scale turbulence.

## 4. Two-way coupling

Ideally, in the study of coupled two-phase flow one would wish to resolve fully the disturbance flow generated by each particle or bubble together with the dynamics of the larger-scale turbulent flow. This is rarely feasible as the particles are often small and below the resolution scale of the turbulent flow calculation. Instead, an approximate representation must be used for the local disturbance flow and a parameterized equation of motion used to calculate the particle motion. An important feature to reproduce is the cumulative effect of the induced disturbance flows of the other particles on the motion of an individual particle. The simplest, approximate way to represent the feedback mechanism of the particle phase on a flow is to represent the particles by a set of point forces acting on the flow, each force being the reaction force to the force of the fluid on the particle. This is the assumption in almost all turbulence models and has been the approach of other studies (Squires and Eaton, 1990; Elghobashi and Truesdell, 1993) of turbulent two-phase flow. It has also been applied extensively in the study of low Reynolds number suspension mechanics, see, for example, Koch (1993). The point-force model is suitable as a first approximation for small particles though it does not adequately take account of the particle size. At this stage however, even the results of point-force methods are still not well understood and it is important to develop these further.

The equations of fluid motion for the numerical simulation are now

$$\frac{D\boldsymbol{u}}{Dt} = -\frac{1}{\rho}\nabla p + \nu\nabla^2\boldsymbol{u} + \sum_{m=1}^{M} \boldsymbol{F}^{(m)}\Delta(\boldsymbol{x} - \boldsymbol{Y}^{(m)}), \tag{8}$$

$$\nabla\cdot\boldsymbol{u} = 0. \tag{9}$$

A total of $M$ particles are included in the flow; $\rho\boldsymbol{F}^{(m)}$ is the resultant force exerted by the $m$th particle on the fluid. The function $\Delta(\boldsymbol{x}-\boldsymbol{Y})$, centered on a particle at $\boldsymbol{Y}(t)$, is the numerical representation of the point force coupling. Eqs. (8) and (9) are solved throughout the whole flow domain, including the volume nominally occupied by the particles; a pseudo-spectral method is again used.

The first point to note is that it is not possible, nor desirable, to have an exact point-force coupling between the particle and fluid phases since the calculation must remain spectrally resolved. Instead, the force is distributed within a narrow envelope $\Delta(\boldsymbol{x} - \boldsymbol{Y})$ centered on the particle position,

$$\Delta(\boldsymbol{x}) = (2\pi\sigma^2)^{-3/2}\exp(-\boldsymbol{x}^2/2\sigma^2). \tag{10}$$

The envelope gives a local spatial average or filtering of the feedback and this can be controlled explicitly by adjusting $\sigma$ relative to the grid spacing. This method has several advantages compared to simple interpolation over neighboring grid points, and may be used in several ways. If $\sigma$ is chosen to be significantly larger than the particle diameter $d$ the envelope $\Delta$ provides a local volume average appropriate for continuum two-fluid models and when summed over all the particles gives a continuously varying, local number density of the particles. If $\sigma$ is significantly smaller than $d$, the point force representation can be extended to include higher-order terms and so give a fully resolved simulation of the particles and their disturbance flow. This is demonstrated for low Reynolds number flows by the results of Saffman (1973) and Patel (1996).

Here we choose $\sigma$ and $d$ to be comparable in scale, localizing the particles of finite size and partially resolving the disturbance flow. If $\Omega_p$ denotes the volume of a particle then in this context an indicator function $\chi$ can be defined for the particle phase

$$0 \leqslant \chi(\boldsymbol{x},t) = \sum_{m=1}^{M} \Omega_p\Delta(\boldsymbol{x} - \boldsymbol{Y}^{(m)}) \leqslant 1. \tag{11}$$

This is a smoothed version of the usual discontinuous indicator function that takes values of 0 or 1 only (Ishii, 1975). A minimum ratio $\sigma/d > 1.3$ is required with the Gaussian envelope (10) to ensure that this indicator function is bounded between 0 and 1, on the assumption also that there is no direct overlap of separate particles. Further the width of the envelope $\sigma$ should be 1.5 times the grid spacing or greater to ensure adequate numerical resolution.

We now consider the equation of particle motion. To focus attention on the effect of individual particles settling under gravity on the flow dynamics we neglect particle inertia and added-mass effects. This is appropriate if the turbulence is relatively weak and the time scales long. The particles then settle (or bubbles rise) at their terminal velocity with a quasisteady balance between fluid drag forces and forces due to gravity. The force exerted, $\rho\boldsymbol{F}^{(m)}$ by each particle is constant. The parameterized equations of particle motion, such as (1) or (4), with one-way coupling reduce to

$$\boldsymbol{V}(t) = \boldsymbol{u}(\boldsymbol{Y},t) + \boldsymbol{W}, \tag{12}$$

where $\boldsymbol{u}(\boldsymbol{Y},t)$ is the ambient flow excluding the local disturbance flow associated with the particle's presence in the flow. This Eq. (12) is equally appropriate at both small and finite particle Reynolds numbers provided the local flow conditions change relatively slowly. Further with particles of small but finite size, a particle will move only in response to fluid motions on scales larger than its own size. Instead of using the fluid velocity at a single point, such as the particle center, the local fluid velocity should be evaluated by again applying the spatial filter or local volume average as

$$\tilde{\boldsymbol{u}}(\boldsymbol{Y},t) = \int \Delta(\boldsymbol{x}-\boldsymbol{Y})\boldsymbol{u}(\boldsymbol{x},t)\,\mathrm{d}^3\boldsymbol{x}. \tag{13}$$

The parameterized equation for particle motion with two-way coupling is instead

$$\boldsymbol{V}(t) = \tilde{\boldsymbol{u}}(\boldsymbol{Y},t) + \boldsymbol{W}', \tag{14}$$

where $\boldsymbol{W}'$ is a modified terminal velocity.

The interpretation of (14) requires some care. The fluid velocity $\tilde{\boldsymbol{u}}$ calculated in (13) from the computed flow field of (8), (9) is, in fact, the sum of two contributions $\tilde{\boldsymbol{u}}^{(1)} + \tilde{\boldsymbol{u}}^{(2)}$. The first, $\tilde{\boldsymbol{u}}^{(1)}$ is the ambient fluid velocity of the turbulence and the flow induced by the other particles, while $\tilde{\boldsymbol{u}}^{(2)}$ is the result of the self-induced disturbance flow and the force coupling centered on $\boldsymbol{Y}(t)$. The magnitude of $\tilde{\boldsymbol{u}}^{(2)}$ in fact scales with $F/\sigma\nu$, so it is sensitive to the choice of the envelope width. In the absence of an ambient flow or other particles the particle should settle with velocity $\boldsymbol{W}$, related to $\boldsymbol{F}$ and dependent on the particle Reynolds number $\mathrm{Re}_\mathrm{p}$ defined by $Wd/\nu$. The particle velocity as given by (14) is then

$$\boldsymbol{V}(t) = \boldsymbol{W} = \boldsymbol{W}' + \tilde{\boldsymbol{u}}^{(2)}. \tag{15}$$

The first thought may be to eliminate $\tilde{\boldsymbol{u}}^{(2)}$ as being extraneous given that a parameterized equation of particle motion is being used, and not a full calculation of the flow around the particle or the fluid forces acting on its surface. However, if $\boldsymbol{u}(\boldsymbol{x},t)$ were indeed the fully resolved flow due to a single particle moving with velocity $\boldsymbol{V}$, then the required boundary condition on the normal velocity component would be $\boldsymbol{V}\cdot\boldsymbol{n} = \boldsymbol{u}\cdot\boldsymbol{n}$ on the particle surface. This condition, together with the fact that flow is incompressible, implies that

$$\Omega_\mathrm{p}\boldsymbol{V} = \int_{\Omega_\mathrm{p}} \boldsymbol{u}(\boldsymbol{x},t)\,\mathrm{d}^3\boldsymbol{x}, \tag{16}$$

irrespective of whether the flow field defined "inside" the particle is a rigid body motion or some other motion. This can be demonstrated by considering the volume integral of $\partial(x_i u_j)/\partial x_j$. A comparison of (10), (11), (13)–(16) indicates that in a fully resolved calculation we would have $\boldsymbol{W}$ equal to $\tilde{\boldsymbol{u}}^{(2)}$, and should then set $\boldsymbol{W}'$ to be zero. On the other hand, if $\tilde{\boldsymbol{u}}^{(2)}$ is eliminated, or negligibly small for instance as the result of assigning a large value to $\sigma$, then $\boldsymbol{W}$ and $\boldsymbol{W}'$ should be set equal to each other.

The relative value of $\boldsymbol{W}'$, or of $\tilde{\boldsymbol{u}}^{(2)}$, to $\boldsymbol{W}$ is thus actually an indicator of the degree to which the disturbance flow of an individual particle has been resolved by the simulation method. In the present example where inertia of the particle is negligible and $\boldsymbol{F}$ is constant these issues are simplified. A constant value can be assigned to $\boldsymbol{W}'$ and the value of $\tilde{\boldsymbol{u}}^{(2)}$ does not vary significantly in any one experiment.

We illustrate these methods with results for particles settling in a homogeneous suspension and then when the particles are embedded in an ambient turbulent flow. The particles are initially distributed at random in a periodic domain with box side, $2\pi$ and (8), (9) and (14) solved for the motion of the fluid and the particles. The particles are identical; the force $\rho \boldsymbol{F}$ on each particle due to gravity is specified by the nondimensional force Reynolds number $\mathrm{Re}_F$, defined as $F/\nu^2$, and $\mathrm{Re}_F = 141$. A total of 10 240 individual particles are introduced and a grid of $128 \times 128 \times 128$ points is used to compute the flow. The force Reynolds number $\mathrm{Re}_F$ is somewhat unconventional but may easily be related to $\mathrm{Re}_p$ for rigid spherical particles in quasisteady motion. In the limit of zero Reynolds number $\mathrm{Re}_F = 3\pi \mathrm{Re}_p$ while for $\mathrm{Re}_F = 141$ the value of $\mathrm{Re}_p$ is approximately 8.4. The effective particle diameter $d$ and volume $\Omega_p$ are then set by $\mathrm{Re}_p$ and the value of $W$ used in the simulations. Larger values of $W$ correspond to smaller, denser particles and hence a stronger influence of the spatial filtering in truncating the high wave number, small scale features of the disturbance flow.

First, we consider the homogeneous suspension of uniformly distributed particles. This flow is generated entirely by the random viscous disturbance flows of the particles. In Table 1 basic statistics of the flow are given with column I referring to the suspension. The average mean flow $\bar{\boldsymbol{u}}$, integrated over the flow domain, is zero throughout the simulation. A mean pressure gradient balances the net weight/buoyancy of the particle phase. The vertical mean square fluid velocity fluctuations $\overline{u_1^2}$ are much larger than those in the horizontal and corresponding to this the vorticity fluctuations in the horizontal are much greater. An individual particle force induces a strong, local axisymmetric vorticity distribution. For low Reynolds numbers conditions this is very similar to that of a Stokes flow or Oseen flow, and is similar to at higher Reynolds number flows for the region outside of the particles. The magnitudes though differ quantitatively due to the spatial filtering of the envelope. As all particles are subject to the same vertical force the effect is cumulative giving an axisymmetric random flow. The particle-mean fluid velocity $\langle \tilde{u}_1 \rangle$ is due primarily to the self-induced disturbance flow. For these simultions a fixed value of $W_1'$ or $\langle V_1 - \tilde{u}_1 \rangle$ is specified, this is 16.0 as may be seen from Table 1. At this chosen mean settling velocity the particle radius is approximately equal to 0.05 or so, and the volume fraction is about 2%, though in this set of data no fluid-phase conditional averages are given. No inertial response time $\tau_p$ or $\tau_B$ is used, and this can be set arbitrarily depending on the density ratio for the particle to the fluid. Just as a comparison with the data in the table a bubble of radius 0.05 in this simulation would have a response time on the order of 0.001 or less.

The particle velocity fluctuations reflect those of the flow, being lower due to the spatial filtering (13). The viscous dissipation rate $\varepsilon$ may be compared with the net rate of working on the fluid by the particle phase $\overline{\boldsymbol{u} \cdot \boldsymbol{f}}$, where

$$\boldsymbol{f}(\boldsymbol{x}, t) = \sum_{m=1}^{M} \boldsymbol{F} \Delta(\boldsymbol{x} - \boldsymbol{Y}^{(m)}(t)). \tag{17}$$

The two are balanced within the limits of statistical error and the slow temporal variation of the flow. In the suspension, the flow is driven by the settling of the particles. The mean pressure gradient does no work overall but cancels $\hat{\boldsymbol{f}}(\boldsymbol{k} = 0, t)$. Integrated over the whole volume,

$$(\overline{\boldsymbol{u} \cdot \boldsymbol{f}})(2\pi)^3 = M \boldsymbol{F} \cdot \langle \tilde{\boldsymbol{u}} \rangle. \tag{18}$$

Spectra for this flow show the contributions from different length scales. Energy spectra $E(k)$ for the flow and $F(k)$ for the particle force $\boldsymbol{f}$ are given in Fig. 4, as functions of $|\boldsymbol{k}|$. The function $E(k)$

Table 1
Flow averages from two-phase flow simulations in computational (unscaled) units

| | I Suspension | II Forced turbulence | III Decaying turbulence |
|---|---|---|---|
| $\overline{u_1^2}$ | 78 | 386 | 132 |
| $(\overline{u_2^2}+\overline{u_3^2})/2$ | 2.9 | 328 | 105 |
| $\overline{\omega_1^2}$ | 49 | 6335 | 2270 |
| $(\overline{\omega_2^2}+\overline{\omega_3^2})/2$ | 2159 | 7673 | 3529 |
| $\varepsilon$ | 1040 | 5162 | 2221 |
| $\overline{\boldsymbol{u}\cdot\boldsymbol{h}}$ | — | 4121 | — |
| $\overline{\boldsymbol{u}\cdot\boldsymbol{f}}$ | 1154 | 881 | 974 |
| $\mathrm{Re}_\lambda$ | 6.9 | 38 | 19.2 |
| $\eta_K$ | 0.06 | 0.04 | 0.05 |
| $\tau_K$ | 0.015 | 0.0068 | 0.01 |
| $v_K$ | 4.0 | 5.9 | 4.8 |
| $\langle V_1\rangle$ | 19.50 | 18.67 | 18.95 |
| $\langle V_1'^2\rangle$ | 65 | 357 | 111 |
| $(\langle V_2'^2\rangle+\langle V_3'^2\rangle)/2$ | 2.5 | 306 | 97 |
| $\langle\tilde{u}_1\rangle$ | 3.50 | 2.67 | 2.95 |
| $\langle\tilde{\omega}_1^2\rangle$ | 22 | 3373 | 1223 |
| $\langle\tilde{\omega}_2^2+\tilde{\omega}_3^2\rangle/2$ | 1131 | 4735 | 2141 |

Flow averages, denoted by overbar, are from the whole domain including the volume occupied by the particle phase; while particle averages, denoted by $\langle\ \rangle$, are averaged over all particles in the domain. Effective Taylor microscale Reynolds number $\mathrm{Re}_\lambda$ is calculated as $(\frac{5}{3})^{1/2}\overline{u_i^2}/(\varepsilon\nu)^{1/2}$, $\nu = 0.238$; $\overline{\boldsymbol{u}\cdot\boldsymbol{h}}$ is mean rate of working per unit mass by the random forcing $\boldsymbol{h}(\boldsymbol{x},t)$, see (6); $\overline{\boldsymbol{u}\cdot\boldsymbol{f}}$ is mean rate of working per unit mass by the particle force coupling $\boldsymbol{f}(\boldsymbol{x},t)$, see (8), (17).

is defined by summing contributions $|\hat{u}_i(\boldsymbol{k},t)|^2$ within spherical shells of radii from $k-\frac{1}{2}$ to $k+\frac{1}{2}$, so that overall

$$\overline{u_i^2} = \int_0^\infty E(k)\,\mathrm{d}k.$$

The other spectra are defined in a corresponding manner. The forcing contributes at intermediate wave numbers, with the spatial filtering of the envelope limiting the influence at high wave numbers. More revealing are the spectra of the energy dissipation $D(k)$, equal here to $\nu k^2 E(k)$, and the spectra $G(k)$ of the force-fluid coupling $\boldsymbol{u}\cdot\boldsymbol{f}$. These are shown in Fig. 5. This shows the close balance of dissipation and particle forcing at high wave numbers. The nonlinear energy transfer spectrum $T(k)$ has the usual features of removing energy from low wave numbers and supplying energy at high wave numbers, but its overall effect is small. At any instant the spectral energy budget for the turbulent kinetic energy is

$$\frac{\partial}{\partial t}\left(\tfrac{1}{2}E(k)\right) = T(k) - D(k) + G(k). \tag{19}$$

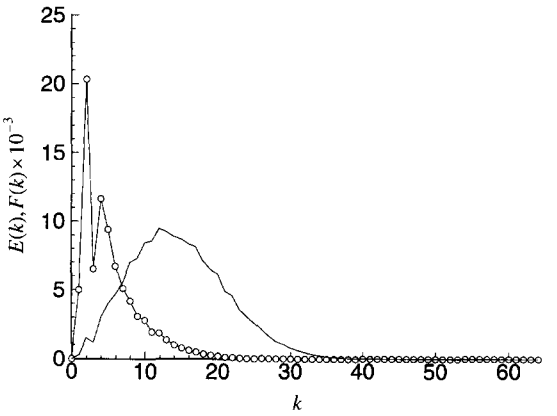


Fig. 4. Energy spectrum function $E(k)$ and particle-force spectrum $F(k)$ for the homogeneous suspension against wave number $k = |\boldsymbol{k}|$; —o—, $E(k)$; ——, $F(k) \times 10^{-3}$.

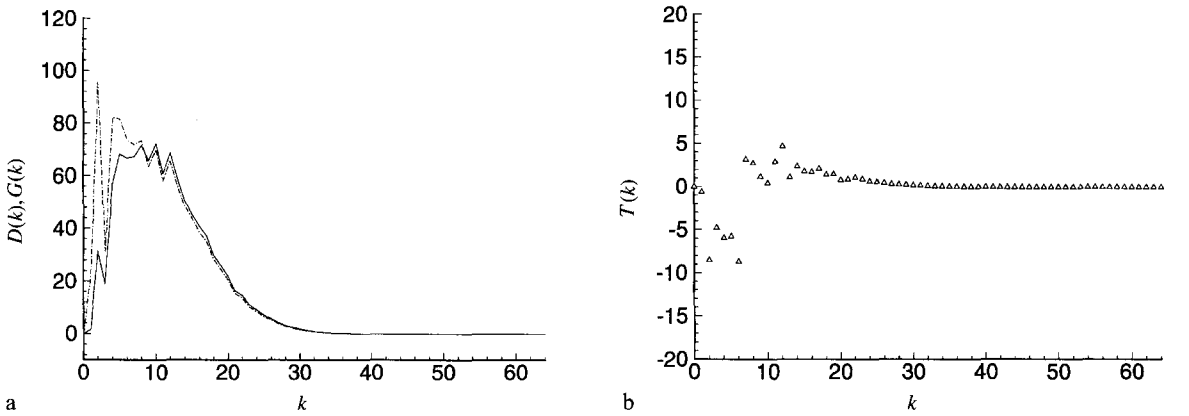


Fig. 5. Energy dissipation spectrum $D(k)$, spectrum function $G(k)$ for the energy input from particle force coupling, and nonlinear energy transfer function $T(k)$ for the homogeneous suspension: (a) ——, $D(k)$; – - - - –, $G(k)$; (b) △, $T(k)$.

Column II of Table 1 gives data for forced homogeneous turbulence some time after the particles have been introduced. In the absence of the particles the turbulence is isotropic. The influence of the particle phase is clear in raising relatively the level of $\overline{u_1^2}$ and the horizontal vorticity components. The energy spectra $E(k)$ shown in Fig. 6, shows a much greater low wave number content in the energy while the forcing spectrum $F(k)$ is quite similar to that of the suspension. The energy dissipation $\varepsilon$ is primarily balanced by the input of the random forcing $\overline{\boldsymbol{u}\cdot\boldsymbol{h}}$ with the particle forcing adding about 20% of the dissipation. The dissipation spectra $D(k)$, Fig. 7, reflects the strong influence of nonlinear energy transfer $T(k)$, especially at low wave numbers. A more detailed comparison, Fig. 8, shows the more noticeable but still smaller effect of $G(k)$ at higher wave numbers.

At this point the random forcing of the turbulence was removed and the turbulence allowed to decay. The effective Reynolds number $\mathrm{Re}_\lambda$ drops by 50% in the time interval and data in column III

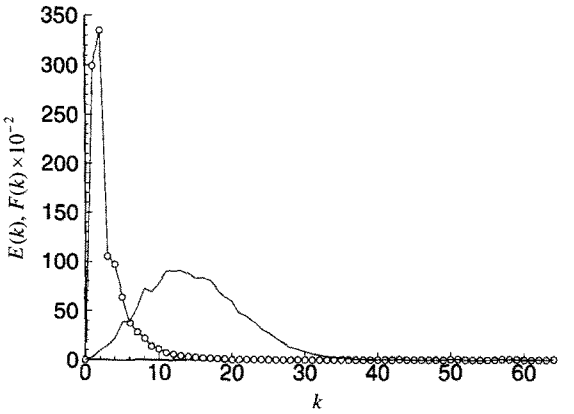


Fig. 6. Energy spectrum $E(k)$ and particle-force spectrum $F(k)$ for forced homogeneous turbulence; —o—, $E(k)$; ——, $F(k) \times 10^{-2}$.

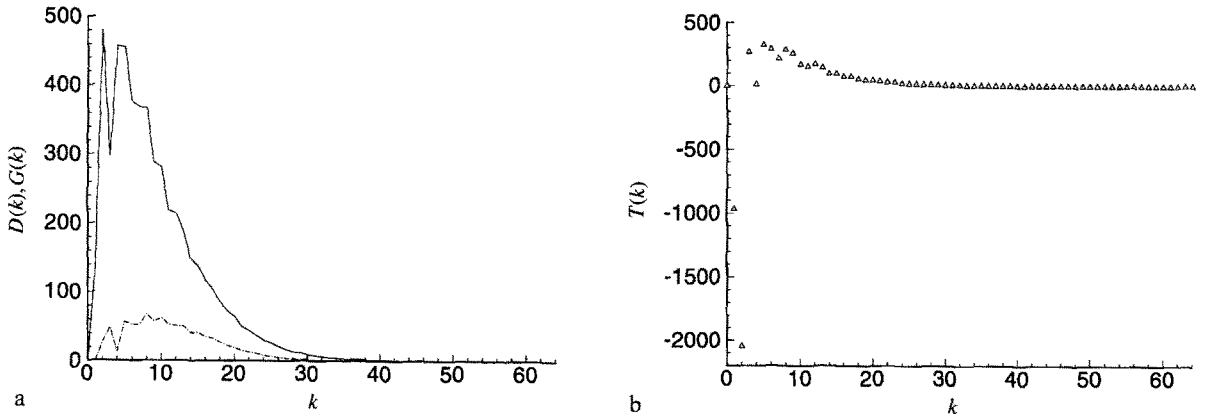


Fig. 7. Energy dissipation spectrum $D(k)$, spectrum function $G(k)$ for energy input from particle force coupling, and nonlinear energy transfer function $T(k)$ for forced homogeneous turbulence: (a) ——, $D(k)$; – – – –, $G(k)$; (b) △, $T(k)$.

of Table 1 give the overall statistics at this stage. The time interval between datasets II and III is 2.0 $T_e$, where $T_e$ is the estimated large-eddy turnover time scale $\overline{u_i^2}/3\varepsilon$ for II. The axisymmetric structure of the turbulence is much more apparent as the forcing from the particle phase has a more significant effect. The dissipation rate $\varepsilon$ is over twice $\overline{\boldsymbol{u}\cdot\boldsymbol{f}}$ and the turbulence continues to decay. The energy spectrum $E(k)$, Fig. 9, is reduced at low wave numbers by the decay process, while $F(k)$ which reflects the spatial distribution of the particles is essentially the same as shown previously. The particle forcing $G(k)$, Fig. 10, now makes a more significant contribution to the balance of energy dissipation and the effect of nonlinear energy transfer $T(k)$ at low wave numbers is much weaker. A comparison at higher wave numbers, Fig. 11, shows the comparable strengths of $T(k)$ and $G(k)$ and in this range as $k$ increases, $D(k)$ is approximately balanced by $T(k) + G(k)$. As the turbulence continues to decay it will revert back to the suspension mode I.

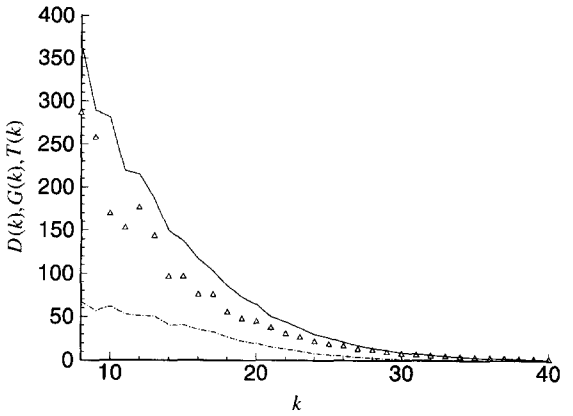


Fig. 8. Same, comparing $D(k)$, $G(k)$, and $T(k)$ for $8 \leqslant k \leqslant 40$.

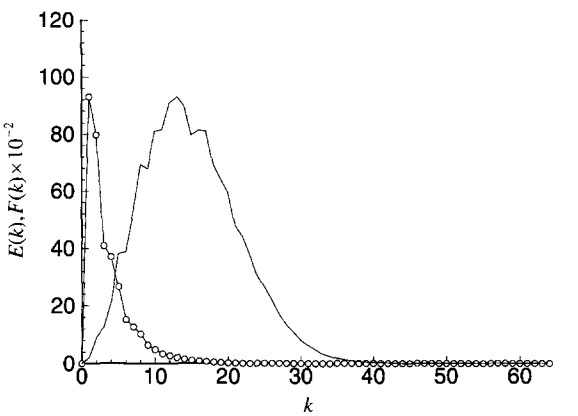


Fig. 9. Same as Fig. 6 for decaying homogeneous turbulence.

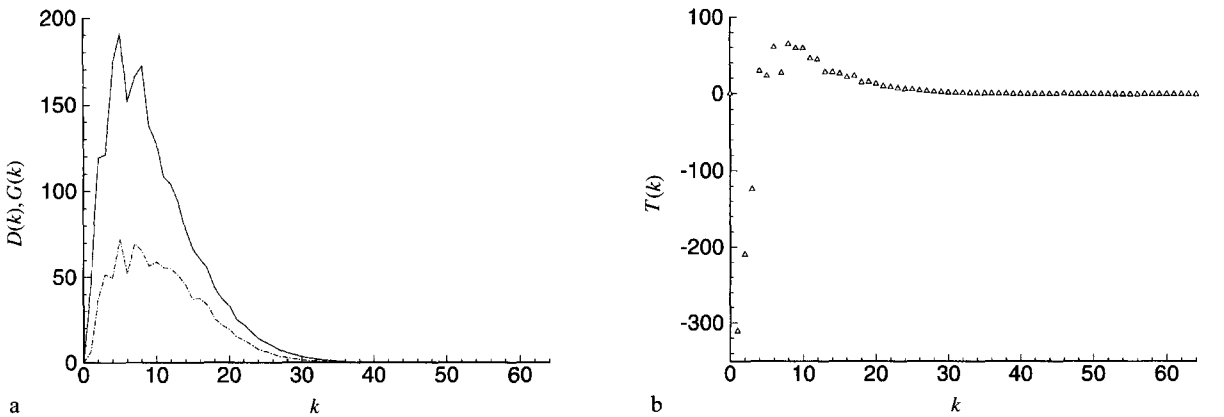


Fig. 10. Same as Fig. 7 for decaying homogeneous turbulence.

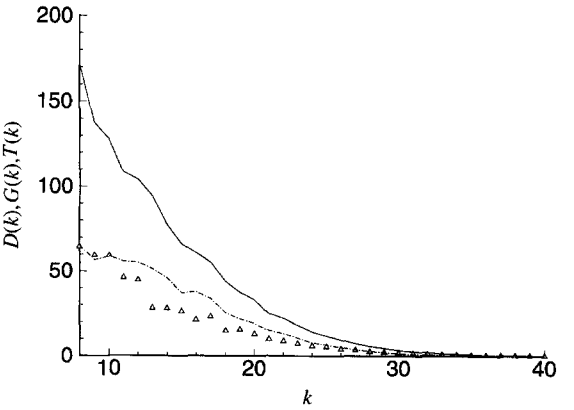


Fig. 11. Same as Fig. 10, comparing $D(k)$, $G(k)$ and $T(k)$ for $8 \leqslant k \leqslant 40$.

## 5. Conclusions

The two-phase flow simulations illustrate the results that particle-force coupled models give, and the degree to which they represent the flow dynamics. The local disturbance flow of each particle generated by the forcing is a strong source of small-scale vorticity that may or may not interact with any ambient turbulent flow. The suspension flow (I) is a random viscous flow that shows a weak nonlinear inertial transfer of energy from low to high wave numbers. The effective value of $\mathrm{Re}_\lambda$ is low and the flow is at most weakly turbulent. This is an example of the pseudo-turbulence referred by Lance and Bataille (1991), though significantly weaker in this case for these small particles. When coupled with an ambient turbulent flow (II) or decaying turbulence (III) the overall effect is to give an axisymmetric rather than isotropic turbulence structure. The influence of the particle phase is more noticeable in the vorticity levels than in the kinetic energy of the flow. In all three examples the particle distribution appears to remain uniform and the values of $F(k)$ and $G(k)$ are quite similar at intermediate and higher wave numbers between the three flows. This suggests that the direct interaction between the turbulence and vorticity generated by the particle phase is limited. A nonuniform particle distribution, as would develop from the influence of particle inertia or added-mass, would produce variations over a larger length scale, or at lower wave numbers, and have a more direct impact on the turbulence kinetic energy.

A second feature to note is that the energy supplied to the flow by the settling particles is given by (18) and is determined by $\boldsymbol{F}\cdot\langle\tilde{\boldsymbol{u}}\rangle$. On the other hand, the rate of working by gravity on the particles is $\boldsymbol{F}\cdot\langle\boldsymbol{V}\rangle$. For a single-particle settling in still fluid, $\langle\boldsymbol{V}\rangle = \boldsymbol{W}$ and the rate of working by gravity is $\boldsymbol{F}\cdot\boldsymbol{W}$. This is completely balanced by the viscous dissipation of the local disturbance flow which generates an equal opposing drag force $-\boldsymbol{F}$ on the particle. For a fully parameterized, two-fluid continuum model the total viscous dissipation is then the sum of the calculated flow dissipation and the dissipation of the unresolved, parameterized disturbance flows associated with the fluid drag forces. The latter is $\boldsymbol{F}\cdot\boldsymbol{W}$ for each particle. The fact that $\boldsymbol{F}\cdot\langle\tilde{\boldsymbol{u}}\rangle$ is nonzero is an indicator that the low wave numbers content of these disturbance flows is being represented by the simulations, albeit approximately, and that $\boldsymbol{F}\cdot\langle\tilde{\boldsymbol{u}}\rangle$ compared to $\boldsymbol{F}\cdot\langle\boldsymbol{V}\rangle$ is a measure of this. In fact, other simulations where $|\langle\boldsymbol{V}-\tilde{\boldsymbol{u}}\rangle|$ is smaller show relatively stronger vorticity and momentum coupling, even where $\boldsymbol{F}$ is unchanged.

Finally, we point out that while the term "particle" has been used in the discussion, the two-phase flow simulations are equally applicable to solid particles in liquids or small, spherical bubbles. Indeed, the main application of the approach described here will be to small particles or bubbles in liquids whose sizes are comparable to the Kolmogorov scales of the turbulence or the computational grid spacing. These may be up to 0.5 or 1 mm in scale for example. Appreciable modification of turbulence requires a moderate to large number of finite-sized particles, giving a void fraction of 1% or so, in this context. For gas–solid flows laden with a large number of very small particles the use of a continuous number density for the particle concentration is appropriate. Other forms of the spatial filter or force envelope (10) may be used too. The Gaussian envelope does have the advantage of being nonnegative both as an envelope in physical space and as a spectral filter. The specification of the envelope is an essential part of the simulation process. These and other issues raised here will be discussed further in future papers.

## Acknowledgements

The support of the National Science Foundation (CTS-9424169), the Office of Naval Research (ONR-N00014-91-J-1340) and the Pittsburgh Supercomputer Center are gratefully acknowledged. The first author wishes to thank the conference organizers and the Ministry of Education, Science and Culture of Japan for the invitation to present this paper at the International Symposium on the Mathematical Modelling of Turbulent Flows, University of Tokyo, December 1995.

## References

Elghobashi, S. and G.C. Truesdell (1992) Direct simulation of particle dispersion in a decaying isotropic turbulence, J. Fluid Mech. 242, 655–700.

Elghobashi, S. and G.C. Truesdell (1993) On the two-way interaction between homogeneous turbulence and dispersed solid particles I: turbulence modification, Phys. Fluids A 5, 1790–1801.

Gore, R.A. and C.T. Crowe (1991) Modulation of turbulence by a dispersed phase, ASME J. Fluids Eng. 113, 304–307.

Ishii, M. (1975) Thermo-Fluid Dynamic Theory of Two-Phase Flow (Eryolles, Paris).

Koch, D.L. (1993) Hydrodynamic diffusion in dilute sedimenting suspensions at moderate Reynolds numbers, Phys. Fluids A 5, 1141–1155.

Lance, M. and J.M. Bataille (1991) Turbulence in the liquid phase of a uniform bubbly air–water flow, J. Fluid Mech. 222, 95–118.

Maxey, M.R., E.J. Chang and L.-P. Wang (1994) Simulation of interactions between microbubbles and turbulent flow, App. Mech. Rev. 47, S70–S74.

Maxey, M.R. and J.J. Riley (1983) Equation of motion for a small rigid sphere in a nonuniform flow, Phys. Fluids 26, 883–889.

Patel, B.K. (1996) Ph.D. Thesis, Division of Engineering, Brown University, Providence, RI, USA.

Riley, J.J. and G.S. Patterson (1974) Diffusion experiments with numerically integrated isotropic turbulence, Phys. Fluids 17, 292–297.

Saffman, P.G. (1973) On the settling speed of free and fixed suspensions, Studies in Appl. Math. LII, 115–127.

Squires, K.D. and J.K. Eaton (1990) Particle response and turbulence modification in isotropic turbulence, Phys. Fluids A 2, 1191–1203.

Squires, K.D. and J.K. Eaton (1991a) Measurements of particle dispersion from direct numerical simulations of isotropic turbulence J. Fluid Mech. 226, 1–35.

Squires, K.D. and J.K. Eaton (1991b) Preferential concentration of particles by turbulence, Phys. Fluids A 3, 1169–1178.

Wang, L.-P. and M.R. Maxey (1993a) Settling velocity and concentration distribution of heavy particles in homogeneous isotropic turbulence, J. Fluid Mech. 256, 27–68.

Wang, L.-P. and M.R. Maxey (1993b) The motion of microbubbles in a forced isotropic and homogeneous turbulence, App. Sci. Res. 51, 291–296.